Impact-parameter dependent stopping powers for axially channeled and semichanneled MeV He ions in GaAs:Er

Y. Kido, A. Ikeda, and Y. Yamamoto
Department of Physics, Faculty of Science and Engineering, Ritsumeikan University, Noji-cho, Kusatsu-shi, Shiga-ken, 525, Japan

J. Nakata
NTT LSI Laboratories, 3-1, Wakamiya, Morinosato, Atsugi-shi, Kanagawa-ken, 243-01, Japan

H. Yamaguchi and K. Takahei
NTT Basic Research Laboratories, 3-1, Wakamiya, Morinosato, Atsugi-shi, Kanagawa-ken, 243-01, Japan
(Received 28 June 1993; revised manuscript received 24 January 1994)

We have investigated the impact-parameter dependence of stopping powers for axially channeled and semichanneled MeV He ions in Er-sheet-doped GaAs epitaxial layers grown by molecular-beam epitaxy. Ion channeling analysis using 2.0 MeV He^+ coupled with the observation by transmission-electron microscope has revealed the formation of fine ErAs clusters, whose lattice constant shrinks and coincides exactly with that of the GaAs host. Thus the Er atoms take the position corresponding to the tetrahedral interstitial site of the GaAs lattice. The Er peak energies in the backscattering spectra strongly depend on the impact-parameter dependent stopping powers, in particular for the incidence along [110] and the directions slightly tilted from [110] and [100]. We divide the stopping power into two parts—contributions from outer electrons and from inner electrons of GaAs. The former is calculated from the dielectric response theory. For the latter, we consider four types of stopping powers dependent upon impact parameter; (1) Dettmann-Robinson theory, (2) the binary-encounter model, (3) the binary encounter combined with the local-density approximation, and (4) the extended-local-electron-density model. The Er peak energies observed are well reproduced employing model (3).

I. INTRODUCTION

Ion channeling is a powerful technique to determine surface and interface structures together with lattice location of dopant atoms. Notable achievements have been made for phase transitions of surface structures, initial growth processes of heteroexpitaxial films, and site location of adsorbed atoms.[1-3] Computer simulation of ion trajectories makes it possible to analyze the channeling spectra precisely and determine the positions of adsorbed and impurity atoms with the accuracy of about 0.1 Å. Within the penetrating depth less than a few thousand Å, any analytic treatments cannot give an accurate ion flux distribution because it is not equilibrated. Thus we should perform Monte Carlo simulation of ion trajectories to obtain accurate atomic structures of near surface regions from the ion channeling spectra. In this case, the precise data of ion-solid interactions are needed such as interatomic potentials and channeling stopping powers in particular their impact-parameter dependence.

In the present work, we have measured the ion channeling spectra from Er-sheet-doped GaAs epitaxial layers grown by molecular beam epitaxy (MBE). First the location of Er is determined exactly from the backscattering yields from Er for [100], [110], and [111] incidences. In the case of channeling and semi-channeling incidences, the peak energy for Er is different from that for the corresponding random incidence. Such Er peak shifts provide the most suitable chance to test the validity of theoretical predictions on electronic stopping powers dependent upon impact parameter.

In order to extract the quantitative information from the channeling spectra, Monte Carlo simulation of ion trajectories is indispensable. We first discuss the simulation method in the context of the accuracy and computing time. The most suitable method should be adopted for the aim of the structure analysis. The simulation is performed to calculate the average energy of He^+ ions and the close encounter probabilities for both lattice and dopant atoms at each atom layer. Then the random and channeling backscattering spectra are easily generated with the above average energies and close encounter probabilities together with the energy spread of backscattered ions calculated from Bohr energy straggling. Thus we can determine precisely the lattice location of Er and also test the models concerning the impact-parameter dependence of the stopping powers for 1.9–2.0 MeV He ions.

Up to now, several experimental works[4-6] have reported upon impact-parameter dependent stopping powers. Dygo and Turos[7] applied the binary collision model based on Lindhard's description[8] to the stopping powers for 2 MeV He^+ ions passing through Si-[100] (Ref. 6) and obtained a satisfactory result. We should note that this stopping powers correspond to the values averaged over impact parameter with respect to Si-[100] string. Bulgakov, Nikolaev, and Shulga[4] and Alkemade, Turkenberg, and Vrijmoeth[5] employed the phenomenological formula given by Oen and Robinson[9] and obtained relatively good agreement with the experimental data for the

100 keV $H^+ \rightarrow NiSi_2/Si(111)$ system. However, this formula includes fitting parameters with physical ambiguity. Dettmann and Robinson[10] calculated the impact-parameter dependent stopping powers for a H^+ projectile based on the time-dependent perturbation theory with first Born approximation. This expression was employed for simulating channeled-ion trajectories,[11-13] although its validity has not been checked experimentally. Recently, Kitagawa[14] derived a simple dielectric function for a nonuniform many-electron gas using the high-frequency approximation. This asymptotic form (local plasmon energy $\ll m v^2$; m is the electron mass, v is the ion velocity) leads to coincidence with the local-density approximation.[15,16] This formula for a one-dimensional change of electron densities was successfully applied to the position-dependent stopping powers of the (100) surfaces of NaCl-type crystals.[17] However, it is considerably difficult to extend this theory to III–V compound semiconductors with covalent bonds.

In this work, we divided the stopping power into two parts, contributions (1) from nonlocalized outer electrons and (2) localized inner electrons. The outer part is calculated from the dielectric response theory assuming a uniform electron density.[18] As the inner part is dependent upon the impact parameter, we consider the following four models: (1) Dettmann-Robinson theory[10], (2) the Lindhard's binary encounter model[8] (BE), (3) the binary encounter combined with the local-density approximation[16] (LB), and (4) the modified-local-electron-density model[19,20] (LEDM). We multiply the inner part by a correction factor to make the sum of the outer part and the inner part averaged over the impact parameter coincide with Ziegler's random stopping power. Their validity is checked by comparing the experimental energy spectra from Er with those calculated using the above theoretical stopping powers.

II. EXPERIMENTAL

The Er-sheet-doped GaAs samples were grown on undoped semi-insulating GaAs (100) substrates by MBE at 500 °C. The detail of sample preparation was described elsewhere.[21,22] The thickness of the epitaxial layers is about 2000 Å. The Er depth profile was determined from a random backscattering spectrum by best fitting the simulated spectrum to the corresponding observed one and is shown in Fig. 1. Here, we assumed joined asymmetric Gaussian shapes as the Er profile.

The samples were mounted on a three-axes goniometer and a well-collimated 2.0 MeV He^+ beam impinged upon the sample with the angular spread of 0.03°. In order to estimate roughly the charge changing cross sections for the channeled He ions, we also utilized a 2.0 MeV He^{2+} beam. The backscattered He ions were detected with a surface barrier detector fixed on a rotatable table in a scattering chamber. The scattering angle was always set at 170°. We determined precisely the detection angle with respect to the incident beam axis by rotating the detector. The beam current on the sample is reduced to zero because of the blocking by the detector holder with a symmetric shape between some rotation angles. The midpoint of the above rotation angles corresponds to the detection angle of 180° with respect to the incident beam axis. The incident ion energies were calibrated using the narrow resonant reactions of $^{27}Al(p,\gamma)^{28}Si$ and $^{27}Al(p,p'\gamma)^{27}Al$ at the proton energies of 991.8 and 1800.0 keV, respectively.[23] The calibration of the energy versus channel number was made by measuring the front edges from Si for 1.0, 1.5, 2.0, and 2.5 MeV He^+ incidence. We estimated the system energy resolution (full width at half maximum) to be 9 keV from the slopes of the front edges of GaAs for random incidence and also from the clearly separated Ga and As surface peaks for channeling incidence (refer to the figures shown in Sec. IV). This means an excellent peak resolution better than 4 keV. Such a low noise level of the detector was realized by making the preamplifier covered thoroughly with Al foils and touched directly with the scattering chamber.

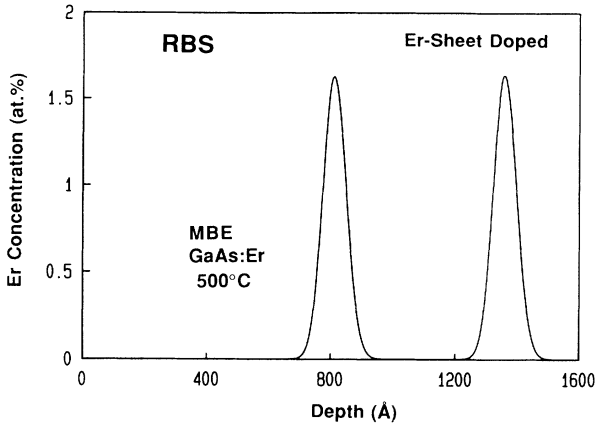

FIG. 1. Er depth profile determined from random backscattering spectrum assuming it to be joined two asymmetric Gaussian shapes.

We set up the perfect channeling ([100], [110], and [111]) and semichanneling (slightly tilted from the major crystal axis) incidences together with the corresponding random incidence by making up the stereo projection diagrams. In order to measure accurate random spectra, a pileup rejection circuit was employed and the beam current was set enough low typically 0.3–0.4 nA. Furthermore, we subtracted the background yields measured with an undoped GaAs crystal from the random spectrum for GaAs:Er. Each energy spectrum was normalized by the integrated beam current of 6.4 μC. We applied a voltage of +200 V onto the sample holder with respect to the scattering chamber to suppress the secondary electron emission. The irradiated area was slightly shifted to avoid contamination buildup and radiation damage on the sample surface. Thus the experimental reproducibility of the backscattering spectra was improved remarkably within several %.

III. SIMULATION OF ION TRAJECTORIES

In this section, we first consider three types of models to simulate ion trajectories: (1) the binary-encounter approximation (BE),[2,24,25] (2) the binary encounter coupled

with multistring model (BE+MS),[7,11-13] and (3) the binary encounter combined with many body potentials (BE+MB). Model (1) is suitable to calculate the flux distributions at the regions not so far from a string and its merit is short computing time. In order to calculate the flux distributions near the channel center accurately, we must take into account the contribution from many neighboring atoms or strings. A continuum string potential is obtained by integrating each atomic potential along the string (z-axis) and, therefore, it has z independence. Thus this continuum potential is a good approximation for calculating the flux distributions at the positions far from the string and those for the ions having traversed long paths. In the present model, the number of strings contributing to the multistring potentials are 16, 12, and 14 for [100], [110], and [111] axes, respectively. In model (3), we consider neighboring lattice atoms interacting with the ion more than ten. Thus this model is the most realistic expression of the potential which a penetrating ion feels. It, however, consumes long computing time.

For describing the atomic configuration of lattices, exact and simplified structures are available. Figure 2 shows the above two models for the zinc-blende-type lattice along [100] and [110] axes. If we consider the structure of atoms located far from the top surface, typically more than 100 atom layer, the simplified model is available. It simplifies the simulation program and reduces the computing time. To analyze a near surface structure accurately, the exact description is indispensable. In the present spectrum simulation, the difference between the above two models is negligibly small.

Next we consider the effect of thermal lattice vibration. Figures 3(a) and 3(b) show the close encounter probabilities for 2.0 MeV He ions traversing along GaAs[100] and [110] strings in which the lattice atoms are static and thermally vibrating. They were calculated with respect to the channel centers and midpoints shown in the insets. Here, we used the BE+MB model and assumed room temperature. The numbers of interacting atoms considered are 16 and 12, for [100] and [110] incidence, respectively. As clearly seen, the effect of thermal vibration is small. This effect becomes significant for calculating flux distributions near a string at higher temperatures.

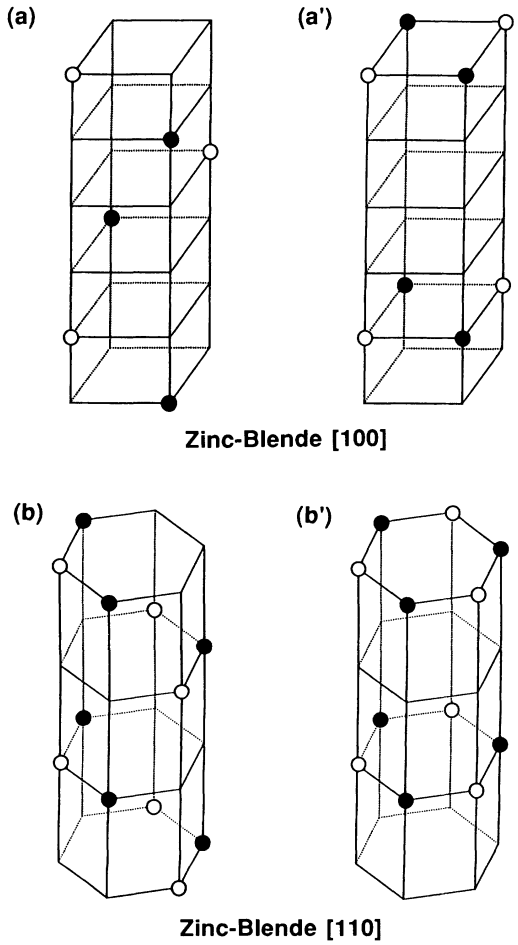

FIG. 2. Unit channels along [100] and [110] axes drawn schematically for zinc-blende-type lattices. (a) and (b) illustrate the exact location of lattice atoms, whereas (a') and (b') show the corresponding simplified configurations.

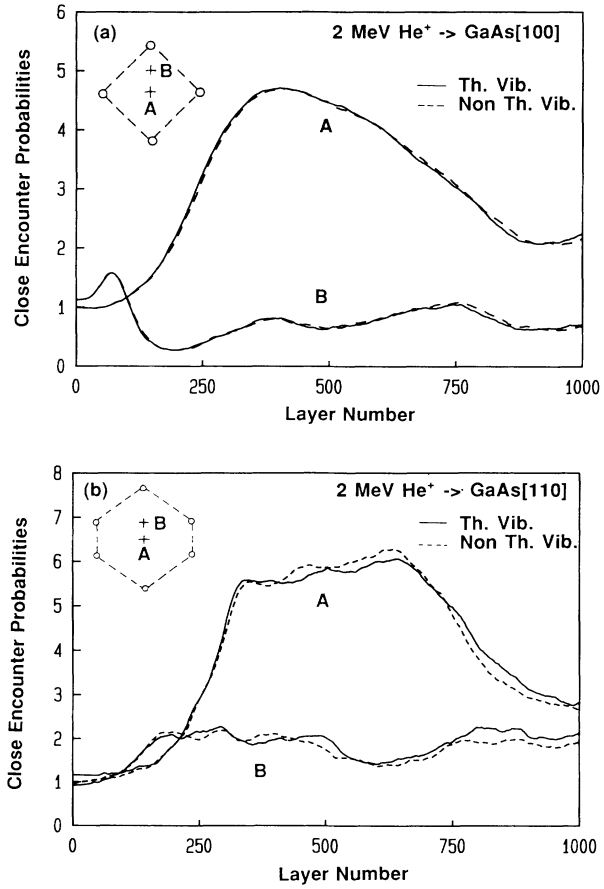

FIG. 3. Close encounter probabilities for 2 MeV He ions incident along GaAs [100] and [110]. It is assumed that dopant atoms locate the lattice positions, A and B shown in each inset. The solid and dashed curves are obtained for thermally vibrating lattice atoms and for static lattice atoms, respectively. Monte Carlo simulation was performed using the BE+MB model considering the interaction potential from neighboring 12 lattice atoms.

Until presently, the Doyle-Turner[26,27] and modified multistring potentials[7,11-13] have been frequently utilized. In the present BE and BE+MS models, however, we consider this effect by generating the position of a collision partner at each atom layer using the normal random number with the standard deviation of two-dimensional thermal vibration amplitude derived from the bulk Debye temperature.

We used the universal potential to express the binary scattering event and to calculate the static multistring potential. This potential has been successfully utilized for H and He ions in a wide energy region,[28,29] Figures 4(a) and 4(b) show the close encounter probabilities for 2.0 MeV He ions passing along GaAS[100] and [110] using the BE, BE+MB, and BE+MS models with respect to the two different lattice positions. Here, we used the exact expression of the lattice structure for the BE and BE+MB models, whereas for the BE+MS model the simplified lattice structure was assumed. In the [100] case, the three models give overall good agreement except for the case using the Lindhard's standard potential to calculate the multistring potential. In the [110] case, the three models give consistent results up to the depth about 200 atom layer but in a deeper region the BE model leads to large deviations from the results obtained using the BE-MS and BE+MB models. We must carefully employ the BE model to calculate the flux distributions for ions having traversed a long path along a major crystal axis with a large area of unit channel. Hereafter, we use the BE+MS model assuming the exact or simplified lattice configuration.

We calculate the normalized close encounter probability, $P_{\mathrm{CL}}(j)$ and the average energy, $E_{\mathrm{AV}}(j)$ for penetrating particles arriving at jth atom layer with respect to the dopant atom locating the lattice position $(X_{\mathrm{dop}}, Y_{\mathrm{dop}})$ in the unit channel (or section). They are defined by

$$P_{\mathrm{CL}}(j)=(A/N_P)\sum_{i=1}^{N_P} f(X_{ij},Y_{ij}) , \tag{1}$$

where

$$f(X_{ij},Y_{ij})=(1/2\pi u_1^2)/\exp[\{X_{\mathrm{dop}}-X_{ij})^2 + (Y_{\mathrm{dop}}-Y_{ij})^2\}/2u_1^2] ,$$

and

$$E_{AV}(j)=\sum_{i=1}^{N_P} E_{ij}f(X_{ij},Y_{ij})\Big/\sum_{i=1}^{N_P} f(X_{ij},Y_{ij}) , \tag{2}$$

where A is the area of the unit channel (or unit section), u_1 is the standard deviation for the distribution of the dopant location, and (X_{ij}, Y_{ij}) is the arrival position at jth atom layer for each channeled or semichanneled particle with an energy E_{ij}. N_P is the number of incident particles, typically 50 000. In the calculation of $P_{\mathrm{CL}}(j)$ and $E_{\mathrm{AV}}(j)$ with respect to the host lattice atoms, $(X_{\mathrm{dop}}, Y_{\mathrm{dop}})$ and u_1 are replaced with an equilibrium position in the string and with one-dimensional thermal vibration amplitude, respectively. For random incidence, all $P_{\mathrm{CL}}(j)$ values are equal to 1.0.

We easily generate both random and channeling backscattering spectra by convoluting each energy spectrum from jth atom layer. It is assumed to be a Gaussian distribution at the modal energy, $E_{\mathrm{AV}}(k,j)$ with its area, $P_{\mathrm{CL}}(k,j)\times Y(k,j)$ and with the standard deviation of $\Omega(k,j)$. Here, k denotes a constituent target element and $Y(k,j)$ and $\Omega(k,j)$ are the random scattering yield calculated from Rutherford scattering cross sections and the energy spread for the particles backscattered from atom, k at the jth atom layer, respectively. For the Er depth profile, we approximated it as joined two asymmetric Gaussian shapes, as mentioned in Sec. II.

IV. IMPACT-PARAMETER DEPENDENCE OF STOPPING POWER

The Er peak shifts provide quantitative information concerning the impact-parameter dependent stopping powers. The LEDM with a solid picture[19,20] has succeeded in calculating random stopping powers of solid media for H and He ions in a wide energy range. Considering the success of this model, we divide the stopping power

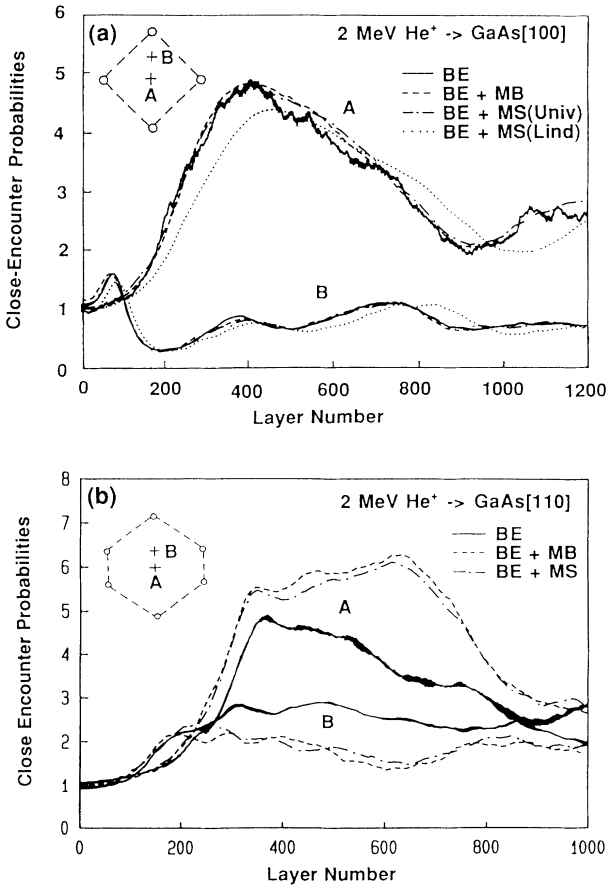

FIG. 4. Close encounter probabilities for 2 MeV He ions incident along GaAs [100] and [110]. Dopant atoms are assumed to locate the lattice positions, A and B shown in each inset. The solid, dashed, and dot-dashed curves are obtained employing the BE, BE+MB, and BE+MS models, respectively. The dotted curve drawn in (a) denotes the result obtained using the multistring potential calculated from the Lindhard's standard potential.

into two parts contributed from nonlocalized outer electrons and from localized inner electrons. The former, $S_{out}(E)$ is expressed by the dielectric response theory which regards a solid as a free-electron gas. It depends only on ion energy E and electron density. Here, the numbers of the outer electrons per atom are three and five for a Ga and As atom, respectively. Thus the homogeneous electron density from outer electrons of GaAs is $4\times N$ electrons/cm^3 (N being the atomic density of GaAs$=4.428\times10^{22}$ atoms/cm^3). $S_{out}(E)$ is proportional to the square of the effective charge (Z_{EF}) of the projectile ions in solids. The effective charge of ions penetrating a solid medium, which cannot be measured directly, has been discussed in the context of stopping powers. Experimental data indicate that the effective charge depends primarily upon the ion velocity and very weakly upon the target atomic number.[21,28] Ziegler, Biersack, and Littmark[29] and Luntz and Bartram[30] proposed the semiempirical formulas for the effective charge of light and heavy ions passing through solid media. The effective charge of ions penetrating a solid medium is different from the mean charge of ions after passing through the medium, because there occurs an electron capture at the exit surface and subsequent rearrangement of the electronic states including Auger electron emission.[31,32] At enough high energies, they become close to the completely stripped charge state. For He energies from 1 to 2 MeV, the formula proposed by Ziegler, Biersack, and Littmark gives significantly higher values than those calculated from the Luntz and Bartram's. As will be shown later, the former gives a too high effective charge to reproduce the experimental [110]-aligned spectra. In the present analysis, we employ the latter expression[30,33] given by

$$Z_{EF}=Z_1[1.0-\exp\{-137.0v/(cZ_1^{2/3})\}] , \tag{3}$$

where Z_1 is the atomic number of the projectile and v and c are the velocities of the projectile and light, respectively.

Now, we consider the contribution from inner electrons, $S_{in}(E,s)$ which is dependent upon impact parameter s. The total electronic stopping power is expressed by

$$S_{tot}(E,s)=S_{out}(E)+c_k S_{in}(E,s) , \tag{4}$$

where c_k is a correction factor determined by making the averaged total stopping power value coincide with the Ziegler's random stopping power $S_Z(E)$.[33] The total stopping power is averaged over s, as follows:

$$\langle S_{tot}(E,s)\rangle_s=S_{out}(E)+c_k/(\pi r_c^2)\int_0^{r_c}2\pi s S_{in}(E,s)ds$$
$$=S_Z(E) . \tag{5}$$

Here, we consider a cylinder with radius $r_c=(\pi Nd)^{-1/2}$ (d being the atomic spacing in a string) and with length d along a major crystal axis. The target atom in a string is located at the center of the cylinder.

The first candidate for the inner part is the DR stopping power[10] based on the Born approximation and derived from the time-dependent perturbation theory. In this case, the c_k value is about 0.8 for 2.0 MeV He ions incident along GaAs[110]. In the present calculation of DR stopping, the projectile charge of +2 was assumed. Thus the above c_k value means the effective charge of +1.8, which is consistent with that derived from Eq. (3).

The second candidate is a binary encounter model proposed by Lindhard.[8] The inner part is further divided into two contributions from close encounter part, $S_{CL}(E,s)$ and distant resonance part, $S_{RS}(E)$. The former (eV/atom) is expressed by

$$S_{CL}(E,s)=[S_B(E)/2]\int_{-\infty}^{+\infty}\rho_e(\sqrt{s^2+z^2})dz , \tag{6}$$

where $\rho_e(r)$ is the electron density in a target atom at a distance r from the nucleus and $S_B(E)$ corresponds to the Bethe-Bloch formula given by

$$S_B(E)=4\pi Z_{EF}^2e^4/(mv^2)\ln(2mv^2/I) . \tag{7}$$

Here, m is the electron mass, e is the electron charge, and I is the mean excitation energy given by $10Z_2$ (Z_2 is the target atomic number). Lindhard regarded the distant resonance part as $S_B(E)/2$ from an equipartion rule, which is valid at enough high energies. We modify the Lindhard model as follows:

$$S_{CL}^{BE}(E,s)=(S_B(E)/2d)\int_{-d/2}^{+d/2}\rho_e(\sqrt{s^2+z^2})dz . \tag{8}$$

Here, the Hartree-Fock-Slater atomic model[35] is used to calculate the above integral. Furthermore, instead of the equipartition rule, we calculate the resonant part for inner electrons, $S_{RS}(E)$ accurately by LEDM, which will be represented later [Eq. (11)].

As the third model, we extend the above close encounter part of the Lindhard's model using the phenomenological local-density approximation[16] as follows (LB-stopping):

$$S_{CL}^{LB}(E,s)=(2\pi Z_{EF}^2e^4/mv^2)(1/d)$$
$$\times\int_{-d/2}^{+d/2}\rho_e(\sqrt{s^2+z^2})$$
$$\times\ln[2mv^2/\hbar\omega_p(\sqrt{s^2+z^2})]dz , \tag{9}$$

where $\hbar$ is the Planck constant and the local plasma frequency $\omega_p(r)$ is defined by

$$\omega_p(r)=[4\pi e^2\rho_e(r)/m]^{1/2} . \tag{10}$$

Apparently, for the inner electrons with large binding energies (> 1 keV) the term in the logarithm becomes lower than unity and produces a negative contribution. In order to avoid such a nonrealistic description, we set an upper limit of 600 eV to $\omega_p(r)\hbar$, which corresponds to the orbital velocity of a bound electron 2.0 times larger than 2 MeV He-ion velocity. For 2.0 MeV He ions traversing along GaAs[110], the c_k values are 1.23 and 1.18 for Ga and As atoms, respectively.

As the fourth candidate for the impact-parameter dependent stopping power of inner electrons, we consider the LEDM, which takes a form,

$$S_{LD}(E)=(4\pi Z_{EF}^2e^4/mv^2)\int_0^{\infty}\rho_e(r)L[\rho_e(r),E]4\pi r^2dr ,$$

(11)

where $L[\rho_e(r),E]$ is the dimensionless stopping number given in an analytic form.[18,19] The stopping number is divided into two parts, close collision term, $L_{\mathrm{CL}}[\rho_e(r),E]$ and distant resonant term, $L_{\mathrm{RS}}[\rho_e(r),E]$. We calculate each term as follows:

$$S_{\mathrm{CL}}^{\mathrm{LD}}(E,s)=(4\pi Z_{\mathrm{EF}}^2 e^4/mv^2) \times \int_s^{\sqrt{s^2+d^2/4}} \rho_e(r) L_{\mathrm{CL}}[\rho_e(r),E]\,4\pi r^2 dr \ , \tag{12}$$

$$S_{\mathrm{RS}}(E)=(4\pi Z_{EF}^2 e^4/mv^2) \times \int_0^{\infty} \rho_e(r) L_{\mathrm{RS}}[\rho_e(r),E]\,4\pi r^2 dr \ . \tag{13}$$

Apparently the above $\{S_{\mathrm{CL}}^{\mathrm{LD}}(E,s)+S_{\mathrm{RS}}(E)\}$ is considerably lower than $S_{\mathrm{LD}}(E)$. In fact, the above formula (MD-LEDM) gives nonrealistic c_k values of 4–5 for Ga and As atoms. It should be noted that in LEDM all the electrons in an atom contribute to the stopping power through both close and distant resonant collisions not in the form averaged over the impact parameter. From a viewpoint of impact-parameter dependence, the simple summation over all electron shells in Eq. (11) seems quite inadequate. Thus, hereafter we omit to apply this model to the simulation of ion trajectories.

Figures 5(a) and 5(b) show the impact-parameter dependent stopping powers of inner electrons calculated from the above four models for Ga and As, respectively. the calculations were made for 2.0 MeV He^+ ions incident along GaAs [110]. In this case, the critical radius r_c of the unit cylinder is 1.34 Å. Each stopping power drawn here is that multiplied by the correction factor, c_k. The DR stopping power decreases relatively slowly with an increase in impact parameter. On the other hand, the BE and LB models give an abrupt decrease with an in-

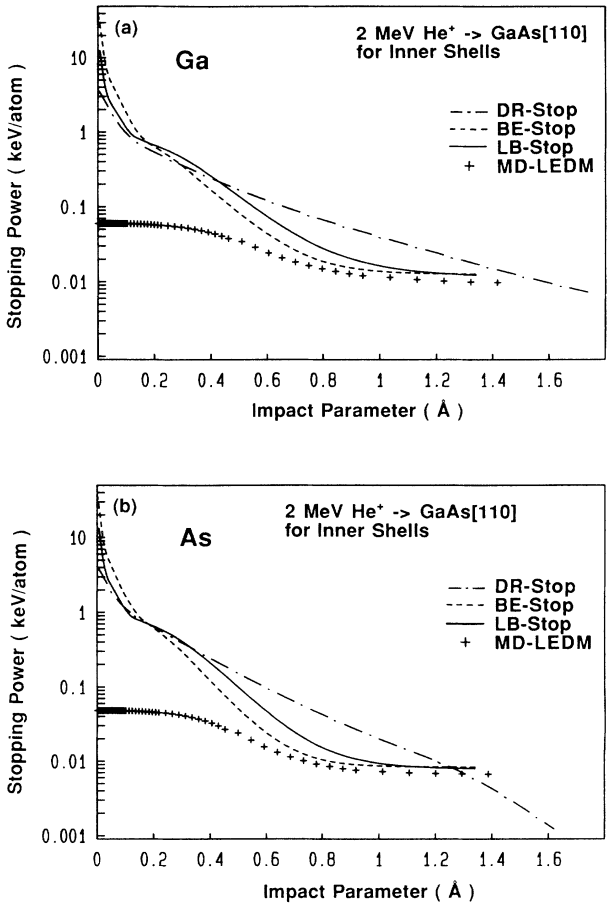

FIG. 5. Impact-parameter dependent stopping powers of inner shell electrons of Ga (a) and As (b) atoms for 2.0 MeV He ions incident along GaAs [110]. The number of inner electrons considered here is 28.

TABLE I. Energy losses of 2.0 MeV He ions incident along GaAs [110] for the lattice positions, *A*, *B*, and *C* at depths 200th and 400th atom layers evaluated from Monte Carlo simulation of ion trajectories. These values are averaged by multiplying the close encounter probabilities with respect to the above three lattice positions. Each value in the parentheses is the ratio of the stopping power for channeling to random incidence (Ziegler's stopping).

Lattice site / Stop. power (eV/Å)	*A* (channel center)	*B* (tetrahedral)	*C* (crystal row)
	200th atom layer		
LB-stop	14.01	14.64	55.48
	(0.44)	(0.46)	(1.76)
BE-stop	14.49	14.95	60.97
	(0.46)	(0.47)	(1.93)
DR-stop	16.40	17.54	59.68
	(0.52)	(0.56)	(1.89)
	400th atom layer		
LB-stop	12.91	13.65	45.38
	(0.41)	(0.43)	(1.44)
BE-stop	13.64	14.76	52.06
	(0.43)	(0.47)	(1.65)
DR-stop	14.63	16.67	45.62
	(0.46)	(0.53)	(1.44)

crease in impact parameter with two steps. The plateau curves in the above two models indicate that the distant resonant part is dominant in the region far from the string, typically more than 1 Å.

Now we apply the DR, BE, and LB models to simulate the ion trajectories and to generate the ion backscattering spectra. Table I shows the calculated energy losses of 2.0 MeV He^+ ions incident along GaAs[110] for the lattice positions, *A* (channel center), *B* (corresponding to the tetrahedral interstitial site), and *C* (string) at the depths, 200th atom layer and 400th atom layer. Each value in the parentheses denotes the ratio of the stopping power for channeled ions to that for random incidence (Ziegler's stopping). With respect to the position *C*, the channeling stopping powers are much larger than random ones, whereas for the positions *A* and *B* the channeling stopping powers are considerably reduced down to 40% of the random ones. The calculated average energy losses of 2.0 MeV He^+ ions incident along GaAs[111] are listed in Table II for the lattice positions *A* (channel center), *B* (midpoint between the center and the string on the short diagonal of the unit channel (rhombus). The area of the [111] unit channel is considerably smaller than that of [110] (hexagon). Therefore, the reduction of the channeled-ion stopping powers is not so large as that in the [110] case.

For the sheet-doped GaAs:Er samples grown by MBE, ion-channeling analysis coupled with TEM observation revealed the formation of fine ErAs (NaCl-type structure) clusters with a spheroidal shape.[22] The cluster size observed by TEM is about 15 Å for the growth temperature of 500 °C. It should be noted that the Er atoms behind the top two atom layers of a cluster are shadowed from the projectile incident along [110]. The lattice constant of the embedded ErAs clusters coincides with that of bulk GaAs, although the lattice constant of the bulk ErAs is about 1.5% larger than that of the bulk GaAs. Thus the location of Er corresponds to the tetrahedral interstitial site of the host lattice. The detailed structure analysis was described elsewhere.[22]

Figure 6(a) shows the random and [110]-aligned backscattering spectra from GaAs:Er. The solid curves are the simulated ones using the LB stopping powers. In order to obtain complete fitting to the observed spectra ([100], [110], and [111]), we assumed the randomly distributed Er fraction of 7% and the existence of surface disorder (oxides) with thickness of about 15 Å. The dechanneling fractions behind the disordered layers were roughly estimated from the following relation:

$$f_d = 2\pi u_1^2 N A(\Delta z/\cos\theta)/A \ , \tag{14}$$

where Δz and θ are the disordered layer thickness and incident angle with respect to surface normal, respectively. The slight deviation at the tail of the second peak is due to the inaccuracy of the Er depth distribution approximated by asymmetric Gaussian shapes. The magnified Er spectra are shown in Fig. 6(b). Both Be and LB stopping powers give good fitting to the experimental aligned spectra, whereas the DR stopping results in Er peak energies about 6 and 8 keV lower than experimental ones for the first and second peaks, respectively. With respect to the tetrahedral interstitial site, the ion flux around 1 Å apart from the nucleus primarly contributes to the close encounter probabilities. Around this region, the primary contribution to the stopping power originates from the outer part and the resonant part from inner electrons with the BE and LB models. Therefore, distinct difference between the BE and LB models is not seen for the [110] incidence [see Figs. 5(a) and 5(b)]. Furthermore, we note that the formula upon the effective charge proposed by Ziegler *et al.* leads to lower Er peak ener-

TABLE II. Energy losses of 2.0 MeV He ions incident along GaAs [111] for the lattice positions *A*, *B*, and *C* at depths 200th and 400th atom layers evaluated from Monte Carlo simulation of ion trajectories. These values are averaged by multiplying the close encounter probabilities with respect to the above three lattice positions. Each value in the parentheses is the ratio of the stopping power for channeling to random incidence (Ziegler's stopping).

Lattice site / Stop. power (eV/Å)	*A* (channel center)	*B* (midpoint)	*C* (crystal row)
	200th atom layer		
LB-stop	17.47	31.01	51.27
	(0.55)	(0.98)	(1.62)
BE-stop	16.79	26.09	65.99
	(0.53)	(0.83)	(2.09)
DR-stop	21.19	34.35	49.71
	(0.67)	(1.09)	(1.57)
	400th atom layer		
LB-stop	17.49	24.03	49.52
	(0.55)	(0.76)	(1.57)
BE-stop	16.87	21.02	41.17
	(0.53)	(0.67)	(1.31)
DR-stop	20.46	28.74	46.33
	(0.65)	(0.91)	(1.47)

gies than the experimental ones, because this formula gives significantly higher effective charges than those calculated from the Luntz and Bartram's formula.

We can expect a significant difference between the BE and LB models if the region from 0.4 to 0.8 Å from the nucleus contributes dominantly to the close encounter probabilities. Thus we made the ion incidence slightly tilted from the major crystal axes. Figures 7(a) and 7(b) show the semialigned-[100] spectra which was measured for the incidence 0.5° off from the [100] axis in the (010) plane. The LB stopping well reproduces the experimental semialgined spectrum. Concerning the second Er peak, the BE model gives the Er peak energy 4–6 keV higher than the experimental one. The DR stopping generates slightly lower Er peak energies than the observed ones. Figures 8(a) and 8(b) show the semialigned-[110] spectra which was measured for the incidence 0.4° off from the [110] axis in the $(1\bar{1}0)$ plane. In this case, the primary contribution is made from the region around 0.8 Å from the nucleus [see Figs. 5(a) and 5(b)]. The LB stopping gives good fitting to the experimental spectrum, whereas the BE stopping generates slightly higher Er peak energies. The DR stopping results in large deviation from the observed Er peak energies toward the low-energy side.

Channeled ions traverse the region with low electron densities. Thus the initial charge state would be conserved until they experience enough large number of electronic collisions. We measured the [110]-aligned spectra using singly and doubly ionized He beams, which are shown in Fig. 9. Here, the best-fitted curve is obtained assuming the LB stopping. No significant difference is seen between the He^+ and He^{2+} incidences. The electron loss cross sections for 2-MeV He ions are estimated to be about 5×10^{-18}cm^2 from the experimental work reported so far.[36,37] Then the mean free path for electron loss is calculated to be about 200 Å, if the ion trajectories are limited to the region 1 Å far from the crystal strings, where the electron densities are less than 2×10^{23} electrons/cm^3. Such a short mean free path does not give a distinct Er peak shift. The present result shows that the charge exchange cross section is the same as the above estimate or higher than it.

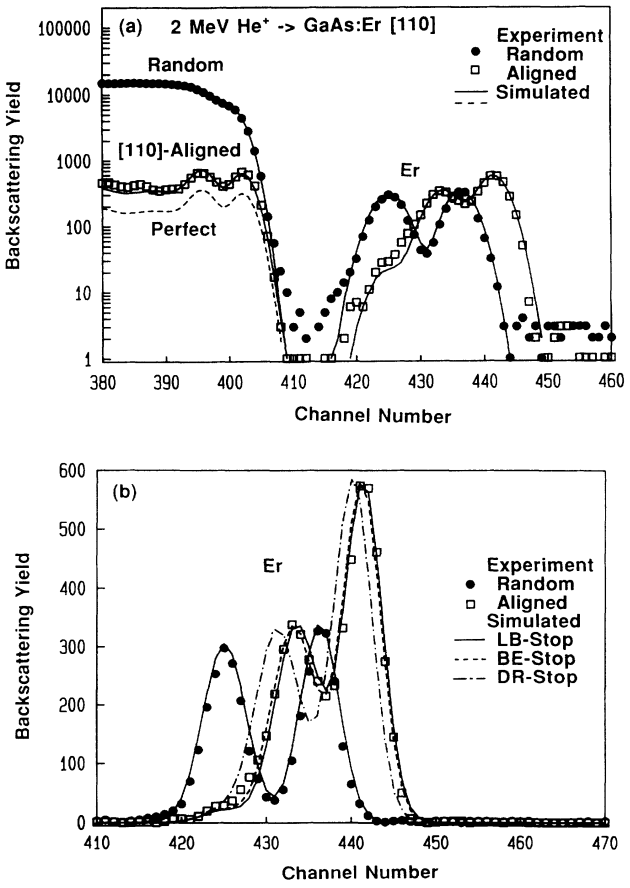

FIG. 6. Observed random (full circles) and [110]-aligned (open squares) spectra from GaAs:Er samples grown at 500°C. Simulation was performed assuming the standard deviation of 0.3 Å for the Er lattice location. The aligned spectra were made up under the assumption that randomly distributed Er fraction is 7% and the visible Er fractions are 100 and 59% for first (surface side) and second peaks, respectively. The magnified Er spectra are shown in (b). Different spectra were obtained employing LB-stopping (solid curve), BE-stopping (dashed curve), and DR-stopping (dot-dashed curve).

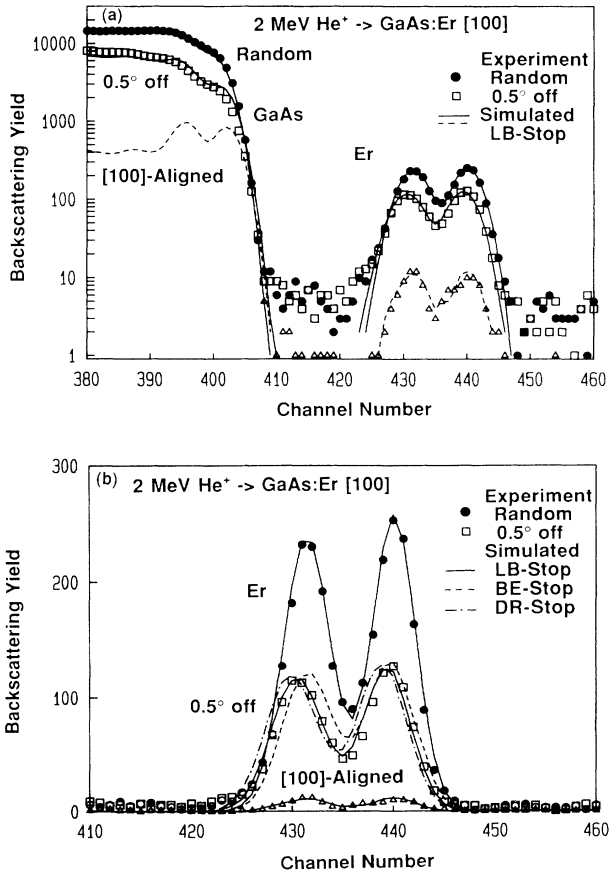

FIG. 7. Observed random (full circles) and semialigned-[100] (open squares) spectra from GaAs:Er. Incident beam axis was tilted by 0.5° from [100] in (010) plane. The magnified Er spectra are shown in (b). Notation is the same as that in Figs. 6.

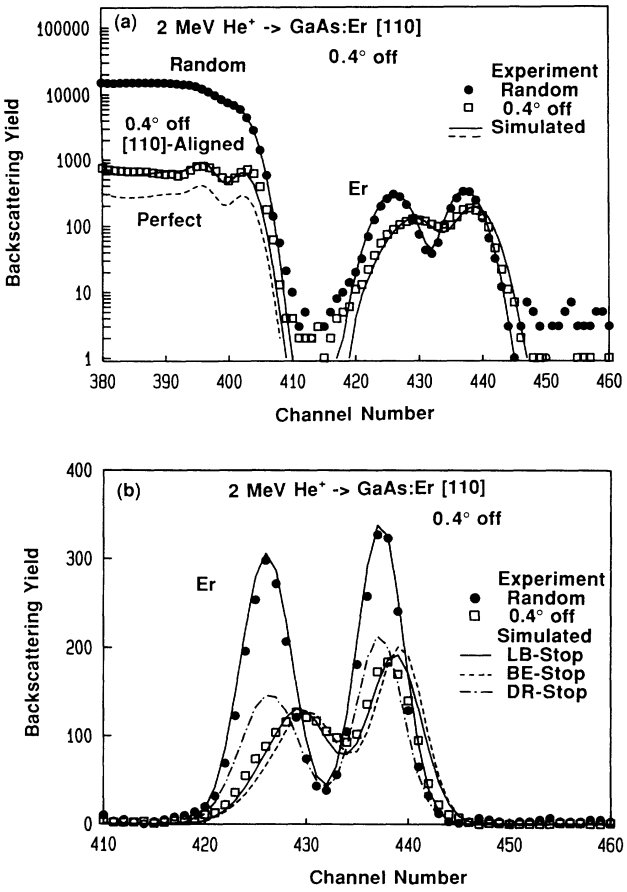

FIG. 8. Observed random (full circles) and semialigned-[100] (open squares) spectra from GaAs:Er. Incident beam axis was tilted by 0.4° from [100] in $(1\bar{1}0)$ plane. Notation is the same as that in Figs. 6.

SUMMARY

We have measured random and aligned (semialigned) backscattering spectra from the Er-sheet-doped GaAs epitaxial layers grown by MBE at 500 °C. Ion channeling coupled with TEM observation has revealed the formation of fine ErAs clusters. Almost all Er atoms take the position corresponding to the tetrahedral interstitial site of the GaAs host lattice.

We have made up three types of Monte Carlo simulation programs to follow ion trajectories; (1) binary-encounter approximation (BE), (2) binary encounter combined with multistring potential (BE+MS), and (3) binary encounter taking account of many-body potentials (BE+MB). The BE+MB model is the most realistic expression of the interaction between the projectile ion and the lattice atoms, although it consumes a long computing time. In the present ion channeling analysis, the BE+MS model was utilized to reduce the computing time without lowering the accuracies.

The Er peak shifts provide the quantitative information upon impact-parameter dependent stopping powers. We divided the electronic stopping power into two parts, contribution from nonlocalized outer electrons and that from localized inner electrons. The former is calculated from the dielectric response theory proposed by Lindhard and Winther.[18] Concerning the effective charge of the projectile in solids, we have checked the validity of two formulas given by Ziegler, Biersack, and Littmark[29] and by Luntz and Bartram.[30] The present experiment and analysis have showed that the former formula gives too high an effective charge to reproduce the experimental Er spectra. For inner electrons, we have proposed four types of stopping powers dependent on impact parameter; (1) Dettmann-Robinson theory (DR), (2) the Lindhard's binary-encounter model (BE), (3) the extended binary-encounter model using the local-density approximation (LB), (4) the modified local density model (LEDM). They are all multiplied by a correction factor to make the total stopping power averaged over the impact coincide with the Ziegler's random stopping power. The present aligned and semialigned Er spectra are well reproduced by employing the LB model coupled with the Luntz and Bartram's formula concerning the effective charge. We have also checked the effect of charge exchange for the channeled-ion stopping powers using singly and doubly ionized He beams. No significant difference in the Er energy spectra was seen between He^+ and He^{2+} beams incident along GaAs[110]. This indicates that the cross sections of charge exchange are larger than 5×10^{-18} cm^2 and is consistent with the experimental data reported by Haruyama *et al.*[36] and by Kimura, Ohtsuki, and Mannami.[37]

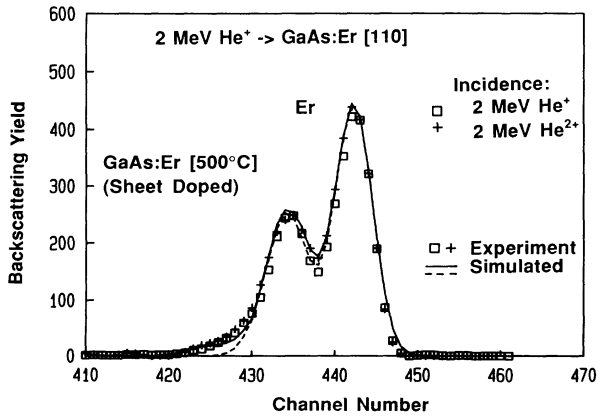

FIG. 9. [110]-aligned spectra from Er of GaAs:Er with He^+ (open squares) and He^{2+} (crosses) beams. Solid curves are the simulated spectra under the same assumption described in the caption of Figs. 6.

ACKNOWLEDGMENTS

We would like to thank Dr. Y. Horikoshi of NTT Basic Res. Lab. for generally supporting our work. Thanks are also due to our colleagues, E. Nakai, T. Ishida, Y. Nakamura, T. Nishimura, and T. Fuse for valuable discussion and providing assistance in computer simulation. We are greatly indebted to Dr. K. Izumi and Dr. K. Murase of NTT LSI Laboratory for realizing our collaboration. This work is partly supported by the Grant-in-Aid for Scientific research on Priority Areas of the Ministry of Education, Science and Culture, Japan.

[1]J. W. M. Frenken and J. F. van der Veen, Phys. Rev. Lett. **54**, 134 (1985).
[2]J. F. van der Veen, Surf. Sci. Rep. **5**, 199 (1985).
[3]L. C. Feldman and J. W. Mayer, *Fundamentals of Surface and Thin Film Analysis* (North-Holland, Amsterdam, 1986).
[4]Yu. V. Bulgakov, V. S. Nikolaev, and V. I. Shulga, Phys. Lett. **46A**, 477 (1974).
[5]P. F. A. Alkemade, W. C. Turkenberg, and J. Vrijmoeth, Nucl. Instrum. Methods B **64**, 716 (1992).
[6]H. S. Jin and W. M. Gibson, Nucl. Instrum. Methods B **13**, 76 (1986).
[7]A. Dygo and A. Turos, Phys. Lett. **127A**, 281 (1988).
[8]J. Lindhard, K. Dan. Vidensk. Selsk. Mat. Fys. Medd. **34**, 14 (1965).
[9]O. S. Oen and M. T. Robinson, Nucl. Instrum. Methods **132**, 647 (1976).
[10]K. Dettmann and M. T. Robinson, Phys. Rev. B **10**, 1 (1974).
[11]P. J. M. Smulders and D. O. Boerma, Nucl. Instrum. Methods B **29**, 471 (1987).
[12]H. Nakano and Y. Kido, J. Appl. Phys. **71**, 133 (1992).
[13]Y. Kido, T. Ishida, E. Nakai, M. Saeki, J. Nakata, and K. Takahei, Nucl. Instrum. Methods B (to be published).
[14]M. Kitagawa, Nucl. Instrum. Methods B **33**, 409 (1988).
[15]J. Lindhard and M. Scharff, K. Dan. Vidensk. Selsk. Mat. Fys. Medd. **27**, 15 (1953).
[16]W. K. Chu and D. Powers, Phys. Lett. **40A**, 23 (1972).
[17]Y. Fujii, S. Fujiawara, K. Narumi, K. Kimura, and M. Mannami, Surf. Sci. **277**, 164 (1992).
[18]J. Lindhard and A. Winther, K. Dan. Vidensk. Selsk. Mat. Fys. Medd. **34**, 4 (1964).
[19]I. Gertner, M. Meron, and B. Rosner, Phys. Rev. A **18**, 2022 (1978).
[20]T. Kaneko, Phys. Rev. A **33**, 1602 (1986).
[21]J. Nakata and K. Takahei, Appl. Phys. Lett. **61**, 2665 (1992).
[22]J. Nakata, K. Takahei, and Y. Kido (unpublished).
[23]G. Deconnick and G. Demortier, J. Radioanal. Chem. **12**, 189 (1972).
[24]R. M. Tromp and J. F. van der Veen, Surf. Sci. **133**, 159 (1983).
[25]J. W. M. Frenken, R. M. Tromp, and J. F. van der Veen, Nucl. Instrum. Methods B **17**, 334 (1986).
[26]P. A. Doyle and P. S. Turner, Acta. Crystallogr. Sec. A **24**, 390 (1968).
[27]L. E. Seibering, P. F. Lyman, and W. M. Grant, J. Vac. Sci. Technol. A **11**, 715 (1993).
[28]H. J. Kang, E. Kawatoh, and R. Shimizu, Jpn. J. Appl. Phys. **23**, L262 (1984).
[29]J. F. Ziegler, J. P. Biersack, and W. Littmark, *The Stopping and Range of Ions in Matter* (Pergamon, New York, 1985).
[30]M. Luntz and R. H. Bartram, Phys. Rev. **175**, 468 (1968).
[31]H. D. Betz, Rev. Mod. Phys. **44**, 465 (1972).
[32]M. C. Cross, Phys. Rev. B **15**, 602 (1977).
[33]J. D. Melvin and T. A. Tombrello, Radiat. Eff. **26**, 113 (1975).
[34]J. F. Ziegler, *Helium Stopping Powers in All Elements* (Pergamon, New York, 1977).
[35]F. Herman and S. Skillman, *Atomic Structure Calculations* (Prentice-Hall, Englewood Cliffs, NJ, 1963).
[36]Y. Haruyama, Y. Kanamori, T. Kido, A. Itoh, and F. Fukuzawa, J. Phys. B **16**, 1225 (1983).
[37]K. Kimura, H. Ohtsuki, and M. Mannami, Phys. Rev. Lett. **68**, 3797 (1992).